Letter

Enhanced hybridization in the electronic ground state of the intercalated honeycomb iridate $Ag_3LiIr_2O_6$

A. de la Torre,[1] B. Zager,[1] F. Bahrami,[2] M. DiScala,[1] J. R. Chamorro,[3,4] M. H. Upton,[5] G. Fabbris,[5] D. Haskel,[5] D. Casa,[5] T. M. McQueen,[3,4,6] F. Tafti,[2] and K. W. Plumb[1,*]

[1]*Department of Physics, Brown University, Providence, Rhode Island 02912, USA*
[2]*Department of Physics, Boston College, Chestnut Hill, Massachusetts 02467, USA*
[3]*Department of Chemistry, Johns Hopkins University, Baltimore, Maryland 21218, USA*
[4]*Institute for Quantum Matter, Department of Physics and Astronomy, Johns Hopkins University, Baltimore, Maryland 21218, USA*
[5]*Advanced Photon Source, Argonne National Laboratory, Argonne, Illinois 60439, USA*
[6]*Department of Materials Science and Engineering, Johns Hopkins University, Baltimore, Maryland 21218, USA*

(Received 10 March 2021; revised 2 September 2021; accepted 10 September 2021; published 22 September 2021)

We use x-ray spectroscopy at the Ir L_3/L_2 absorption edge to study powder samples of the intercalated honeycomb magnet $Ag_3LiIr_2O_6$. Based on x-ray absorption and resonant inelastic x-ray scattering measurements, and exact diagonalization calculations including nearest-neighbor Ir-Ir electron hopping integrals, we argue that the intercalation of Ag atoms results in a delocalized electronic structure with enhanced Ir-O hybridization, departing from the local relativistic $j_{\text{eff}} = 1/2$ state. We find that the relative orbital contribution to the magnetic moment is increased and the magnetization density is spatially extended and asymmetric in this hybridized state. Our results confirm the importance of metal-ligand hybridization in the magnetism of transition metal oxides and provide empirical guidance for understanding the collective magnetism in intercalated honeycomb iridates.

DOI: 10.1103/PhysRevB.104.L100416

Recognition that the Kitaev model, an exactly soluble quantum spin liquid, may have material realization in heavy transition metal oxides has driven significant research for the past decade [1]. The emergence of this effective quantum compass model depends on a hierarchy of crystal field, spin-orbit coupling, and electronic correlations that act to generate a relativistic atomic orbital basis with $j_{\text{eff}} = 1/2$ effective angular moments. For insulators with edge-sharing octahedra coordinating $j_{\text{eff}} = 1/2$ ions, isotropic Heisenberg exchange interactions nearly vanish and the magnetism is dominated by spatially anisotropic Kitaev exchange [1]. On the other hand, *ab initio* calculations find that for many model $j_{\text{eff}} = 1/2$ materials, kinetic energy can promote Ir-O-Ir hybridization and the formation of a quasimolecular orbital (QMO) state [2,3]. In this delocalized scenario the Kitaev model is not obviously applicable and little is known about the collective magnetism.

In the context of Heisenberg-Kitaev magnetism, there has been intensive research on honeycomb iridates [4–6] and α-$RuCl_3$ [7–9]. These compounds have strong Kitaev exchange in addition to Heisenberg and pseudodipolar interactions that result in magnetic order [10,11]. A successful strategy to reduce Néel temperatures has been to synthesize new versions of these compounds by substitution on the alkali site through intercalation between the honeycomb planes, for example, $Ag_3LiIr_2O_6$ and $H_3LiIr_3O_6$ [12–14]. However, the $j_{\text{eff}} = 1/2$ state is fragile against structural details [15,16] while bond disorder and off-stoichiometries can inhibit magnetic order [17,18]. An empirical understanding of the influence of chemical substitutions on this state is lacking and there does not yet exist a sound starting point to understand collective magnetism in these intercalated materials.

In this Letter, we use x-ray spectroscopies to show that the topochemical exchange of interlayer Li atoms with Ag in $Ag_3LiIr_2O_6$ [19–21] enhances Ir-O hybridization and fundamentally alters the magnetism. X-ray absorption reveals that the magnetism in $Ag_3LiIr_2O_6$ is characterized by an asymmetric spin density with strong spin-orbit coupling and a larger orbital component than the parent compound α-Li_2IrO_3. Resonant inelastic x-ray scattering (RIXS) spectra probing the Ir electronic structure of $Ag_3LiIr_2O_6$ is captured by incorporating strong Ir-O hybridization, demonstrating that the local $j_{\text{eff}} = 1/2$ picture is not a valid basis. $Ag_3LiIr_2O_6$ must be understood as a new type of delocalized model quantum magnet. We posit that similar effects may be at play in other intercalated honeycomb iridates. Our results provide an empirical foundation to develop suitable effective Hamiltonians in these next-generation frustrated magnets.

High crystalline quality powder samples of $Ag_3LiIr_2O_6$, $T_N = 8$ K, and α-Li_2IrO_3 were from the same clean batch as in [19]. Samples of $Sr_3CaIr_2O_9$ were prepared as described in [22]. RIXS was performed at Sector 27 (MERIX) at the Advanced Photon Source (APS) of the Argonne National Laboratory [23]. We used a horizontal $2\theta = 90^\circ$ scattering geometry, with a 2 m radius spherically diced Si(844) analyzer to give a 33 meV overall energy resolution (full width at half maximum, FWHM). Powder diffraction was conducted at APS 11-ID-B using a wavelength of 0.2115 Å and a sample-to-detector distance of 167.335 mm, calibrated with a ceria standard. The 2D diffraction data were integrated using GSAS-II and then corrected and normalized

*Corresponding author: kemp_plumb@brown.edu

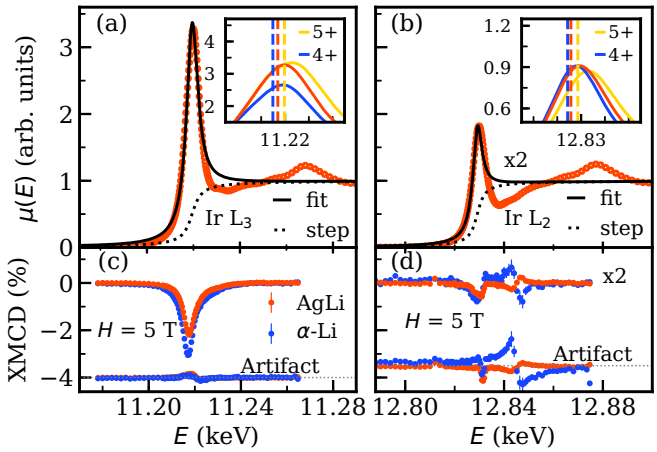

FIG. 1. (a), (b) Ir L_3 and L_2 edge XAS at $T = 300$ K. Black line is a fit, as explained in the main text. Insets in (a) and (b) detail L_3 and L_2 white lines for $Ag_3LiIr_2O_6$, Li_2IrO_3 (Ir^{4+}), and $Sr_3CaIr_2O_9$ (Ir^{5+}). Dashed lines mark the inflection points. (c), (d) $H = 5$ T and $T = 1.6$ K XMCD data for $Ag_3LiIr_2O_6$ and α-Li_2IrO_3. The magnitude of the spurious contributions due to experimental artifact is shown. XAS and XMCD data at the L_2 edge are scaled by a factor of two for clarity.

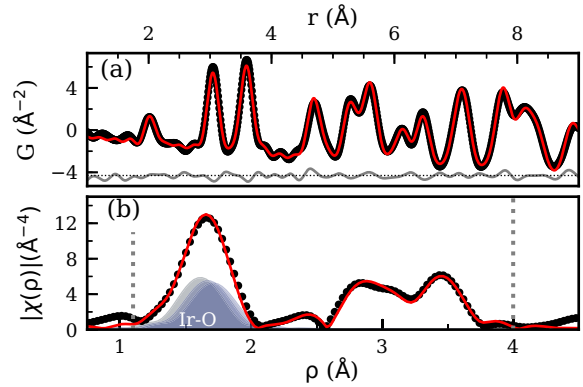

FIG. 2. (a) Atomic PDF at $T = 300$ K; red line is a refinement in the range $r = 1.2$–12 Å and gray line is difference between refinement and data. (b) Magnitude of the Fourier transform of $T = 300$ K EXAFS oscillations and fit (red line). Shaded gray regions indicate the contribution from Ir-O bonds.

to obtain the atomic pair distribution function (PDF), $G(r)$, using PDFgetX3 [24]. X-ray absorption near edge structure (XANES), far edge (EXAFS), and x-ray magnetic circular dichroism (XMCD) were performed in transmission at APS 4-ID-D. XAS and EXAFS data were analyzed using the Larch [25] and FEFF [26] software packages. Magnetic field and temperature were controlled using a 6.5 T liquid He cooled magnet system. XMCD circular polarization was generated using a 500 μm diamond phase plate.

In Figs. 1(a) and 1(b) we show the normalized absorption intensity at the Ir L_3 and L_2 edge, respectively. Both the relative position of the L_3 white line inflection points and the L-edge sum rules provide quantitative information on the oxidation state of a transition metal ion [27–29]. To extract this information, we fit the normalized data to an arctangent step and Lorentzian peak [30]. The results of our analysis are summarized in Table I. The inset of Fig. 1 shows a direct comparison of the white line measured in $Ag_3LiIr_2O_6$, α-Li_2IrO_3 ($5d^5$), and $Sr_3CaIr_2O_9$ ($5d^4$) [22]. In $Ag_3LiIr_2O_6$, we find $\langle n_h \rangle = 5.5(2)$ by averaging the results obtained from white line inflection points and integrated intensities. This deviates from $\langle n_h \rangle = 5$ expected for a localized $j_{\text{eff}} = 1/2$ state [21]. We also find a branching ratio, $\text{BR} = I_{L_3}/I_{L_2} = 5.7(4)$, that is comparable to that of α-Li_2IrO_3, confirming that spin-orbit coupling is a dominant energy scale in $Ag_3LiIr_2O_6$ [3,31,32].

TABLE I. Summary of the parameters extracted from the analysis of the $L_{3,2}$ XAS data.

Material ($\langle n_h \rangle$)	L_3 (eV)	$I(L_3) + I(L_2)$	BR	$\langle L \cdot S \rangle$
α-Li_2IrO_3 (5)	11219.0	22.0(5)	5.0(4)	2.5(2)
$Ag_3LiIr_2O_6$ (5.5)	11219.4	26.0(5)	5.7(4)	3.1(2)
$Sr_3CaIr_2O_9$ (6)	11220.0	30.0(5)	6.5(5)	3.6(2)

If the hole concentration extracted from the XAS analysis is interpreted to arise from a Ir^{4+}/Ir^{5+} mixture, it implies that 50% of the Ir are in a nonmagnetic $j = 0$ state. Such a large fraction of Ir^{5+} is not consistent with chemical analysis or the measured paramagnetic moment of $\mu_{\text{eff}} = 1.87\ \mu_B$/Ir [19] and our XAS measurements at the Ag L_3 edge, that rule out Ag in the 0+ oxidation state [21]. Moreover, we find a six orders of magnitude reduction in low-temperature resistivity of $Ag_3LiIr_2O_6$ compared with α-Li_2IrO_3 [21]. Thus, the more plausible explanation is that the increased electronegativity of Ag over Li results in a larger inductive effect on Ir, effectively bringing Ir away from half filling and increasing the Ag electron count with respect to the +1 oxidation state in the ionic limit. This is consistent with an increase in Ir-O hybridization in $Ag_3LiIr_2O_6$ when compared to α-Li_2IrO_3 as found by LDA+U calculations [33].

Metal ligand hybridization is known to affect the magnetism in transition metal oxides [34–37]. We performed XMCD at the Ir $L_{3,2}$ edges with $H = 5$ T and $T = 1.6$ K in order to understand the influence of the charge redistribution on the magnetism [Figs. 1(c)–1(d)]. XMCD measures the projection of the magnetic moment along the x-ray helicity, set to be parallel to the magnetic field direction. We find that the XMCD signal at the L_3 edge is reduced in $Ag_3LiIr_2O_6$ compared with α-Li_2IrO_3. This may be related to a reduction in the on-site Ir moment, or to differences in the in-field magnetic structure between these two compounds. We apply XMCD sum rules to find orbital $\langle L_z \rangle$, spin $\langle S_z \rangle$, and intra-atomic magnetic dipole moment T_z contributions [38–40]. For a single $j_{\text{eff}} = 1/2$ hole one expects $\langle L_z \rangle / 2\langle S_z \rangle = 2$ [41]. Small departures from the ideal values arising from noncubic crystal fields and covalency are common in iridates [42–44], but we find even larger differences for $Ag_3LiIr_2O_6$. Sum rule analysis using the measured $\mu(H = 5\ \text{T}) \approx 0.05\ \mu_B$/Ir moment for α-Li_2IrO_3 [45] gives $\langle L_z \rangle = -0.028(1)\ \mu_B$/Ir, $\langle S_z \rangle = -0.011\ \mu_B$, and $\langle L_z \rangle / 2\langle S_z \rangle = 1.27$ and $7\langle T_z \rangle / 2\langle S_z \rangle = 1$. For $Ag_3LiIr_2O_6$ we find $\langle L_z \rangle = -0.018(3)\ \mu_B$/Ir and $\langle S_z \rangle = -0.002(3)\ \mu_B$, using $\langle n_h \rangle = 5.5(2)$ and the measured moment of $\mu(H = 5\ \text{T}) = (\langle L_z \rangle + 2\langle S_z \rangle) = 0.022(5)\ \mu_B$ [19,21]. These values

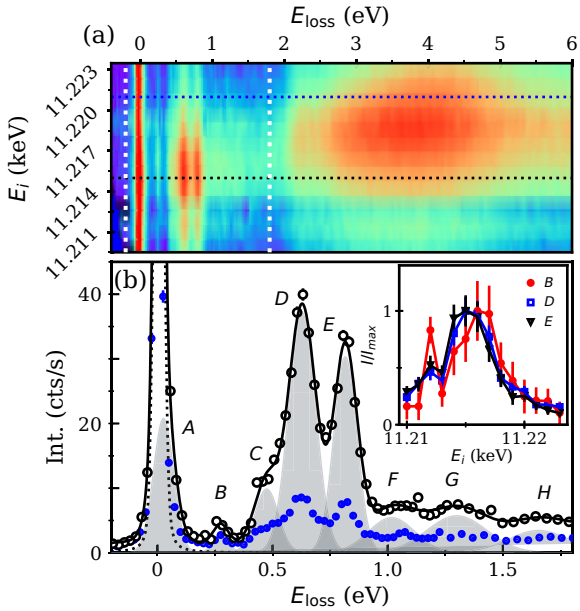

FIG. 3. (a) Ir L_3 RIXS intensity as a function of E_i and $E_{\rm loss}$ in $Ag_3LiIr_2O_6$ at $T = 20$ K. Vertical dotted lines indicate the$E_{\rm loss}$ range for (b). Horizontal dotted lines are color coded according to the RIXS spectrum in (b). (b) Representative RIXS spectrum at $E_i = 11.215$ keV (black markers) and fit to the data (black solid line) with Gaussian peaks (gray shaded) and Voigt elastic line (dotted), as described in the main text. Blue markers show the RIXS spectrum at $E_i = 11.221$ keV. Inset shows the integrated intensity of features B, D, and E as a function of E_i.

lead to $\langle L_z\rangle/2\langle S_z\rangle = 2.6$–$4.5$ and $7\langle T_z\rangle/2\langle S_z\rangle = 1.85$–$6.15$. The minimum twofold enhancement of the fractional contribution of $\langle L_z\rangle$ to the total moment in $Ag_3LiIr_2O_6$ further rules out Ir^{5+} $j = 0$ states where $\langle L_z\rangle/2\langle S_z\rangle = 0.5$ and establishes the orbital nature of magnetism.

Large values of T_z are associated with aspherical spin density originating from noncubic fields, spin-orbit coupling, and electron delocalization due to metal-ligand hybridization [46–48]. To quantify departures from a cubic Ir environment, we carefully examined the local structures of $Ag_3LiIr_2O_6$ using x-ray PDF and EXAFS measurements (Fig. 2). Both measurements are independently consistent with the reported $C2/m$ space group [14] over a broad r range. We find distortions of the Ir environment, with Ir-O distances ranging from 2.021 to 2.119 Å, and Ir-O-Ir bond angles of 92.38° and 95.72° [21]. While the associated trigonal fields in $Ag_3LiIr_2O_6$ are larger than in α-Li_2IrO_3, the 5% difference in Ir-O bond distance is not enough to account for the minimum 80% enhancement of $7\langle T_z\rangle/2\langle S_z\rangle$. We thus assign differences in the magnetism of $Ag_3LiIr_2O_6$ to an increased delocalization of the Ir $5d$ electrons over the ligands [47].

Having found that the magnetism in $Ag_3LiIr_2O_6$ is characterized by a more delocalized electron density, we performed RIXS measurements to better understand the Ir electronic structure. Figure 3(a) shows the $T = 20$ K RIXS signal in $Ag_3LiIr_2O_6$ as a function of incident energy, E_i, and energy transfer, $E_{\rm loss}$. Thompson scattering has a vanishing cross section in our 90° scattering configuration; thus any phonon contribution to the RIXS signal is minimal. The broad and intense features centered at $E_{\rm loss} \approx 3.8$ eV originate from $t_{2g} \rightarrow e_g$ transitions, consistent with the strong crystal field limit, $10Dq > 3$ eV [16,49–51]. For the remainder of this work, we concentrate on the intra-t_{2g} excitations, $E_{\rm loss} \leqslant 1.5$ eV. Figure 3(b) shows a representative RIXS spectrum of $Ag_3LiIr_2O_6$ at $E_i = 11.215$ keV. In order to analyze the experimental data, we fit eight Gaussian peaks: $A = 0.029(25)$, $B = 0.270(37)$, $C = 0.470(60)$, $D = 0.623(69)$, $E = 0.811(58)$, $F = 1.010(109)$, $G = 1.300(153)$, $H = 1.654(150)$ eV and include a resolution-limited Voigt function for the elastic line [21]. The RIXS spectrum of $Ag_3LiIr_2O_6$ is distinct from an ideal local $j_{\rm eff} = 1/2$ state, where only a single excitation between the $j = 3/2$ quartet and $1/2$ doublet appears at $\Delta E = 3\lambda/2 \approx 0.75$ eV, where λ is the spin orbit coupling constant. $\Delta E_{D-E} = 0.19(4)$ eV is larger than the corresponding 0.11(3) eV splittings in α-Li_2IrO_3 and Na_2IrO_3 [50], consistent with a more trigonally distorted environment. However, noncubic crystal fields cannot reconcile the RIXS spectra with a single-site Ir^{4+} model that can at most produce two RIXS features for $E_{\rm loss} < 1$ eV [21].

The energy of A, $E^A_{\rm loss} = 29$ meV, is consistent with collective magnetic excitations observed in other iridates [52–56]. We find that the intensity of peak A follows detailed balance, but there is no correlation with the Curie-Weiss temperature ($\theta_{\rm CW} = -132$ K) [19], ruling out a spin wave origin [21]. Peak C, $E^C_{\rm loss} = 470$ meV, is suggestive of the electron-hole exciton in Na_2IrO_3, α-Li_2IrO_3, and Sr_2IrO_4 [50,57]. Peak B, $E^B_{\rm loss} = 0.279$ eV, is more puzzling. A similar feature in other Ir^{4+} compounds was associated with Ir^{5+} impurities based on qualitative arguments, but the relative intensity of this feature rules out an origin from the <1% off-stoichiometries in our sample, as constrained by chemical analysis [19,21].

Our XAS and XMCD measurements indicate strong Ir-O hybridization in $Ag_3LiIr_2O_6$. Thus, we consider a quasilocal model including trigonal fields and hopping integrals between nearest-neighbor Ir atoms in the large cubic crystal field limit ($t_\parallel$, $t_{\rm O}$, t_σ, $t_\perp$). We follow the labels and hopping paths described in Ref. [3]. These hopping terms are akin to those discussed for the QMO state [2,3,36,58]. We note that our nearest-neighbor model is the minimal unit for electron delocalization and is a realistic approximation that captures hybridization-related splitting of single-ion levels [51]. We fix $\lambda = 0.395$ eV, on-site Coulomb interaction, $U = 2$ eV, and Hund's coupling, $J_H = 0.3$ eV, [21,51]. In Figs. 4(a)–4(c), we show the resulting energy spectrum from exact diagonalization calculations as a function of the dominating t_{2g} hopping integrals $t_\parallel$, hopping between orbitals in parallel plane, and $t_{\rm O}$, O 2_p mediated hopping, and noncubic crystal fields, δ. The dashed horizontal lines and shaded boxes indicate the centroids and FWHM of peaks A–G. We parametrize the energy difference between the calculated excitonic spectrum and the experimental peak positions through a *quality factor*, QF [21], minimized across δ, $t_\parallel$, $t_{\rm O}$, $t_\sigma = -t_\parallel$, and $t_\perp = -0.05t_\parallel$. Measured RIXS spectra can be reproduced within our model for the parameter set $t_{\rm O} = 0.525(13)$ eV, $-0.18 < t_\parallel < -0.07$ eV, and $-0.07 < \delta < -0.02$ eV with a 10% variation of QF from the minimum [21]. Density functional theory calculations find $t_\parallel/t_{\rm O} \approx 0.1$ in $H_3LiIr_2O_6$

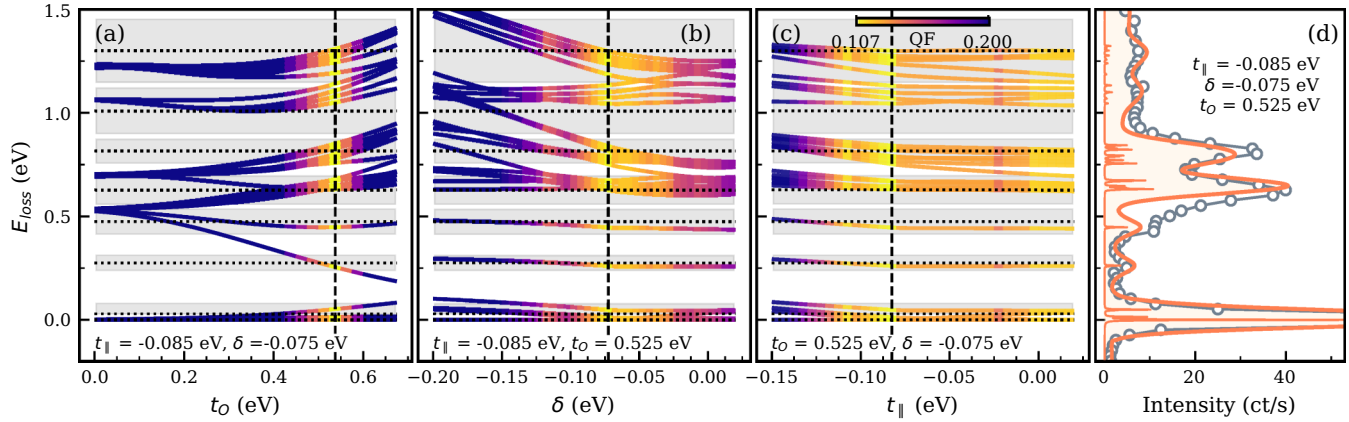

FIG. 4. Calculated energy spectrum of $Ag_3LiIr_2O_6$ as a function of (a) t_O, (b) δ, and (c) $t_\parallel$ with $\lambda = 0.395$ eV, $U = 2$ eV, $J_H = 0.3$ eV, $t_\sigma = -t_\parallel$, and $t_\perp = -0.05t_\parallel$. Horizontal dashed line and gray boxes represent the center energy and FWHM of the extracted inelastic peaks. The color map indicates agreement of the calculation with the experimental data as encoded by the quality factor (QF). (d) Simulated RIXS spectrum for the best parameters compared to the measured intensity.

[18]; thus, we fix $t_\parallel$ to the lower end of the range consistent with our data. False color maps in Figs. 4(a)–4(c) show the dependence of the QF around a set of parameters within this range. Using the optimized parameters—$t_O = 0.525$ eV, $t_\parallel = -0.085$ eV, and $\delta = -0.075$ eV—we computed the powder-averaged RIXS intensity over the three inequivalent bond directions [18,21,59] and convolved with a Gaussian profile (FWHM = 33 meV) to compare with our data in Fig. 4(d).

We can account for all observed $E_{\rm loss} < 1.5$ eV RIXS peaks, including peaks A, B, C, F, and G which the single-ion model fails to capture, by including electron hopping and noncubic crystal fields. In particular, peak B is strongly dependent on t_O. This hopping term is inversely proportional to the energy difference between Ir t_{2g} and O $2p$ orbitals, and *ab initio* calculations have shown that it depends on the intercalated ion. In $H_3LiIr_2O_6$, hybridization of the H $1s$ and O $2p$ orbitals enhances $t_O = 0.3$–0.4 eV [18] with respect to that of Na_2IrO_3 ($t_O = 0.270$ eV) [2,3]. It is plausible that the larger spatial extent of Ag orbitals compared with Li, increased electronegativity, and the energy overlap of Ag and O states [14] enhances the hybridization between Ir-O already present in the parent compound [60] and leads to the larger t_O in $Ag_3LiIr_2O_6$. This is consistent with the measured temperature dependence of the resistivity, which although still displaying insulating behavior is orders of magnitude smaller than that of the parent compound [21]. On the other hand, including further neighbor terms [37] and/or a larger J_H, within the physical meaningful range $J_H = 0.2$–0.4 [61], may reduce the value of t_O that can still explain our data [21]. Similar effects could be at play in $H_3LiIr_2O_6$ and we find that hybridization-related RIXS features should be resolvable for values of $t_O > 0.2$ eV, within expectations for that compound. Finally, we compute the expectation values associated with L and S by calculating the eigenvalues of L^2 and S^2 associated with the projection of the eigenvectors resulting from the exact diagonalization into the associated orthonormal basis. We find an enhancement of the orbital contribution to the ground state of the quasilocal two-site model $[L(L+1)]/[S(S+1)] = 2.99$, when compared to the expected $j_{\rm eff} = 1/2$ state $[L(L+1)]/[S(S+1)] = 2.66$. This demonstrates consistency between our RIXS and XMCD results.

The delocalized magnetic state in $Ag_3LiIr_2O_6$ has important implications for the magnetism of intercalated iridates. In $Ag_3LiIr_2O_6$, the paramagnetic moment $\mu_{\rm eff} = 1.87\ \mu_B$/Ir [14,19] agrees with the expected 1.74 μ_B/Ir for $j_{\rm eff} = 1/2$. Muon spin resonance measurements also find oscillations characteristic of incommensurate magnetic order, similar to that of α-Li_2IrO_3, hinting at a common origin of the magnetism [19,37]. Our finding of an asymmetric spin density and large orbital contribution warrants a more nuanced interpretation. The fundamental magnetic unit in $Ag_3LiIr_2O_6$ is an extended and anisotropic electron density over Ir and O sites [62] that will promote long-range and possibly anisotropic interactions. The result is a greater magnetic frustration with enhanced Curie-Weiss ($\theta_{\rm CW} = -132$ K vs $\theta_{\rm CW} = -105$ K), but reduced ordering temperatures from the parent α-Li_2IrO_3 [14,19]. Thus, hybridization could offer another possible route to spin liquids in iridates. The spatially extended spin density also has consequences for neutron scattering measurements, as the magnetic form factor of such a state will depart from the localized limit. In order to interpret magnetic measurements and design future materials more closely approaching the quantum spin liquid limit, more detailed studies of the effective magnetic Hamiltonians for such a delocalized state are needed [18].

In summary, we have used a suite of x-ray spectroscopies to find that intercalation of Ag atoms on inter-honeycomb-layer sites in α-Li_2IrO_3 promotes Ir-O hybridization and alters the magnetism. Our data and analysis reveal that the electronic structure $Ag_3LiIr_2O_6$ is delocalized, a result of a more trigonally distorted Ir environment and enhanced hopping integrals. The magnetism is characterized by an asymmetric spin density and large orbital moment that is drastically different from the parent compound. As a result, magnetic frustration is enhanced indicating that delocalization may offer an alternative route to spin liquids in the iridates. This phenomenology may extend to other intercalated versions of the honeycomb iridates and our results provide a foundation to develop effective magnetic Hamiltonians for these compounds.

We thank M. Dean for helpful discussions and for his critical reading of this manuscript. Work at Brown University was supported by the U.S. Department of Energy, Office of Science, Office of Basic Energy Sciences, under Award No. DE-SC002165. The work at Boston College was supported by the National Science Foundation under Award No. DMR-1708929. T.M.M. and J.R.C. acknowledge support from the Institute for Quantum Matter, an Energy Frontier Research Center funded by the U.S. Department of Energy, Office of Science, Office of Basic Energy Sciences, under Award No. DE-SC0019331. Use of the Advanced Photon Source at Argonne National Laboratory was supported by the U.S. Department of Energy, Office of Science, Office of Basic Energy Sciences, under Contract No. DE-AC02-06CH11357.

[1] G. Jackeli and G. Khaliullin, Phys. Rev. Lett. **102**, 017205 (2009).
[2] I. I. Mazin, H. O. Jeschke, K. Foyevtsova, R. Valentí, and D. I. Khomskii, Phys. Rev. Lett. **109**, 197201 (2012).
[3] K. Foyevtsova, H. O. Jeschke, I. I. Mazin, D. I. Khomskii, and R. Valentí, Phys. Rev. B **88**, 035107 (2013).
[4] J. Chaloupka, G. Jackeli, and G. Khaliullin, Phys. Rev. Lett. **105**, 027204 (2010).
[5] Y. Singh and P. Gegenwart, Phys. Rev. B **82**, 064412 (2010).
[6] Y. Singh, S. Manni, J. Reuther, T. Berlijn, R. Thomale, W. Ku, S. Trebst, and P. Gegenwart, Phys. Rev. Lett. **108**, 127203 (2012).
[7] K. W. Plumb, J. P. Clancy, L. J. Sandilands, V. V. Shankar, Y. F. Hu, K. S. Burch, H.-Y. Kee, and Y.-J. Kim, Phys. Rev. B **90**, 041112(R) (2014).
[8] A. Banerjee, J. Yan, J. Knolle, C. A. Bridges, M. B. Stone, M. D. Lumsden, D. G. Mandrus, D. A. Tennant, R. Moessner, and S. E. Nagler, Science **356**, 1055 (2017).
[9] A. Banerjee, C. A. Bridges, J.-Q. Yan, A. A. Aczel, L. Li, M. B. Stone, G. E. Granroth, M. D. Lumsden, Y. Yiu, J. Knolle, S. Bhattacharjee, D. L. Kovrizhin, R. Moessner, D. A. Tennant, D. G. Mandrus, and S. E. Nagler, Nat. Mater. **15**, 733 (2016).
[10] J. G. Rau, E. K.-H. Lee, and H.-Y. Kee, Phys. Rev. Lett. **112**, 077204 (2014).
[11] J. G. Rau and H.-Y. Kee, arXiv:1408.4811.
[12] M. Abramchuk, C. Ozsoy-Keskinbora, J. W. Krizan, K. R. Metz, D. C. Bell, and F. Tafti, J. Am. Chem. Soc. **139**, 15371 (2017).
[13] K. Kitagawa, T. Takayama, Y. Matsumoto, A. Kato, R. Takano, Y. Kishimoto, S. Bette, R. Dinnebier, G. Jackeli, and H. Takagi, Nature (London) **554**, 341 (2018).
[14] F. Bahrami, W. Lafargue-Dit-Hauret, O. I. Lebedev, R. Movshovich, H.-Y. Yang, D. Broido, X. Rocquefelte, and F. Tafti, Phys. Rev. Lett. **123**, 237203 (2019).
[15] I. I. Mazin, S. Manni, K. Foyevtsova, H. O. Jeschke, P. Gegenwart, and R. Valentí, Phys. Rev. B **88**, 035115 (2013).
[16] J. P. Clancy, H. Gretarsson, J. A. Sears, Y. Singh, S. Desgreniers, K. Mehlawat, S. Layek, G. K. Rozenberg, Y. Ding, M. H. Upton, D. Casa, N. Chen, J. Im, Y. Lee, R. Yadav, L. Hozoi, D. Efremov, J. van den Brink, and Y.-J. Kim, npj Quantum Mater. **3**, 35 (2018).
[17] R. Yadav, R. Ray, M. S. Eldeeb, S. Nishimoto, L. Hozoi, and J. van den Brink, Phys. Rev. Lett. **121**, 197203 (2018).
[18] Y. Li, S. M. Winter, and R. Valentí, Phys. Rev. Lett. **121**, 247202 (2018).
[19] F. Bahrami, E. M. Kenney, C. Wang, A. Berlie, O. I. Lebedev, M. J. Graf, and F. Tafti, Phys. Rev. B **103**, 094427 (2021).
[20] A. Chakraborty, V. Kumar, S. Bachhar, N. Büttgen, K. Yokoyama, P. K. Biswas, V. Siruguri, S. Pujari, I. Dasgupta, and A. V. Mahajan, Phys. Rev. B **104**, 115106 (2021).
[21] See Supplemental Material at http://link.aps.org/supplemental/10.1103/PhysRevB.104.L100416 for detailed characterization of the measured samples, additional details about the exact diagonalization calculations, further information about the analysis and fitting of the XAS data, temperature dependence of XAS spectra and RIXS spectra, details of the EXAFS and pair distribution refinements, comparison of the magnetic moment and XMCD signal as a function of magnetic field, and direct comparison of RIXS data for Ir^{4+} and Ir^{5+} compounds, which includes Refs. [63–73].
[22] D. C. Wallace and T. M. McQueen, Dalton Trans. **44**, 20344 (2015).
[23] Y. Shvyd'ko, J. Hill, C. Burns, D. Coburn, B. Brajuskovic, D. Casa, K. Goetze, T. Gog, R. Khachatryan, J.-H. Kim, C. Kodituwakku, M. Ramanathan, T. Roberts, A. Said, H. Sinn, D. Shu, S. Stoupin, M. Upton, M. Wieczorek, and H. Yavas, J. Electron Spectrosc. Relat. Phenom. **188**, 140 (2013).
[24] P. Juhás, T. Davis, C. L. Farrow, and S. J. L. Billinge, J. Appl. Crystallogr. **46**, 560 (2013).
[25] M. Newville, J. Phys.: Conf. Ser. **430**, 012007 (2013).
[26] J. J. Rehr, J. J. Kas, M. P. Prange, A. P. Sorini, Y. Takimoto, and F. Vila, C. R. Phys. **10**, 548 (2009).
[27] F. M. F. de Groot, J. C. Fuggle, B. T. Thole, and G. A. Sawatzky, Phys. Rev. B **42**, 5459 (1990).
[28] J. P. Clancy, N. Chen, C. Y. Kim, W. F. Chen, K. W. Plumb, B. C. Jeon, T. W. Noh, and Y.-J. Kim, Phys. Rev. B **86**, 195131 (2012).
[29] M. A. Laguna-Marco, P. Kayser, J. A. Alonso, M. J. Martínez-Lope, M. van Veenendaal, Y. Choi, and D. Haskel, Phys. Rev. B **91**, 214433 (2015).
[30] C. Donnerer, M. M. Sala, S. Pascarelli, A. D. Rosa, S. N. Andreev, V. V. Mazurenko, T. Irifune, E. C. Hunter, R. S. Perry, and D. F. McMorrow, Phys. Rev. B **97**, 035106 (2018).
[31] G. van der Laan and B. T. Thole, Phys. Rev. Lett. **60**, 1977 (1988).
[32] S. Calder, G.-X. Cao, S. Okamoto, J. W. Kim, V. R. Cooper, Z. Gai, B. C. Sales, M. D. Lumsden, D. Mandrus, and A. D. Christianson, Phys. Rev. B **89**, 081104(R) (2014).
[33] A. Nag, S. Bhowal, M. M. Sala, A. Efimenko, I. Dasgupta, and S. Ray, Phys. Rev. Lett. **123**, 017201 (2019).
[34] V. V. Mazurenko, I. V. Solovyev, and A. A. Tsirlin, Phys. Rev. B **92**, 245113 (2015).
[35] S. V. Streltsov and D. I. Khomskii, Proc. Natl. Acad. Sci. USA **113**, 10491 (2016).
[36] S. V. Streltsov and D. I. Khomskii, Phys. Usp. **60**, 1121 (2017).
[37] S. M. Winter, Y. Li, H. O. Jeschke, and R. Valentí, Phys. Rev. B **93**, 214431 (2016).

[38] B. T. Thole, P. Carra, F. Sette, and G. van der Laan, Phys. Rev. Lett. **68**, 1943 (1992).

[39] P. Carra, B. T. Thole, M. Altarelli, and X. Wang, Phys. Rev. Lett. **70**, 694 (1993).

[40] C. T. Chen, Y. U. Idzerda, H.-J. Lin, N. V. Smith, G. Meigs, E. Chaban, G. H. Ho, E. Pellegrin, and F. Sette, Phys. Rev. Lett. **75**, 152 (1995).

[41] B. J. Kim, H. Jin, S. J. Moon, J.-Y. Kim, B.-G. Park, C. S. Leem, J. Yu, T. W. Noh, C. Kim, S.-J. Oh, J.-H. Park, V. Durairaj, G. Cao, and E. Rotenberg, Phys. Rev. Lett. **101**, 076402 (2008).

[42] D. Haskel, G. Fabbris, M. Zhernenkov, P. P. Kong, C. Q. Jin, G. Cao, and M. van Veenendaal, Phys. Rev. Lett. **109**, 027204 (2012).

[43] M. A. Laguna-Marco, G. Fabbris, N. M. Souza-Neto, S. Chikara, J. S. Schilling, G. Cao, and D. Haskel, Phys. Rev. B **90**, 014419 (2014).

[44] S. Agrestini, C.-Y. Kuo, K. Chen, Y. Utsumi, D. Mikhailova, A. Rogalev, F. Wilhelm, T. Förster, A. Matsumoto, T. Takayama, H. Takagi, M. W. Haverkort, Z. Hu, and L. H. Tjeng, Phys. Rev. B **97**, 214436 (2018).

[45] S. Choi, S. Manni, J. Singleton, C. V. Topping, T. Lancaster, S. J. Blundell, D. T. Adroja, V. Zapf, P. Gegenwart, and R. Coldea, Phys. Rev. B **99**, 054426 (2019).

[46] J. Stöhr, J. Magn. Magn. Mater. **200**, 470 (1999).

[47] E. Goering, A. Bayer, S. Gold, G. Schütz, M. Rabe, U. Rüdiger, and G. Güntherodt, Phys. Rev. Lett. **88**, 207203 (2002).

[48] D. Schmitz, C. Schmitz-Antoniak, A. Warland, M. Darbandi, S. Haldar, S. Bhandary, O. Eriksson, B. Sanyal, and H. Wende, Sci. Rep. **4**, 5760 (2014).

[49] X. Liu, V. M. Katukuri, L. Hozoi, W.-G. Yin, M. P. M. Dean, M. H. Upton, J. Kim, D. Casa, A. Said, T. Gog, T. F. Qi, G. Cao, A. M. Tsvelik, J. van den Brink, and J. P. Hill, Phys. Rev. Lett. **109**, 157401 (2012).

[50] H. Gretarsson, J. P. Clancy, X. Liu, J. P. Hill, E. Bozin, Y. Singh, S. Manni, P. Gegenwart, J. Kim, A. H. Said, D. Casa, T. Gog, M. H. Upton, H.-S. Kim, J. Yu, V. M. Katukuri, L. Hozoi, J. van den Brink, and Y.-J. Kim, Phys. Rev. Lett. **110**, 076402 (2013).

[51] Y. Wang, R. Wang, J. Kim, M. H. Upton, D. Casa, T. Gog, G. Cao, G. Kotliar, M. P. M. Dean, and X. Liu, Phys. Rev. Lett. **122**, 106401 (2019).

[52] J. Kim, J. Chaloupka, Y. Singh, J. W. Kim, B. J. Kim, D. Casa, A. Said, X. Huang, and T. Gog, Phys. Rev. X **10**, 021034 (2020).

[53] A. Revelli, M. Moretti Sala, G. Monaco, C. Hickey, P. Becker, F. Freund, A. Jesche, P. Gegenwart, T. Eschmann, F. L. Buessen, S. Trebst, P. H. M. van Loosdrecht, J. van den Brink, and M. Grüninger, Phys. Rev. Research **2**, 043094 (2020).

[54] H. Gretarsson, J. P. Clancy, Y. Singh, P. Gegenwart, J. P. Hill, J. Kim, M. H. Upton, A. H. Said, D. Casa, T. Gog, and Y.-J. Kim, Phys. Rev. B **87**, 220407(R) (2013).

[55] A. Ruiz, N. P. Breznay, M. Li, I. Rousochatzakis, A. Allen, I. Zinda, V. Nagarajan, G. Lopez, Z. Islam, M. H. Upton, J. Kim, A. H. Said, X.-R. Huang, T. Gog, D. Casa, R. J. Birgeneau, J. D. Koralek, J. G. Analytis, N. B. Perkins, and A. Frano, Phys. Rev. B **103**, 184404 (2021).

[56] S. H. Chun, P. P. Stavropoulos, H.-Y. Kee, M. M. Sala, J. Kim, J.-W. Kim, B. J. Kim, J. F. Mitchell, and Y.-J. Kim, Phys. Rev. B **103**, L020410 (2021).

[57] J. Kim, M. Daghofer, A. H. Said, T. Gog, J. van den Brink, G. Khaliullin, and B. J. Kim, Nat. Commun. **5**, 4453 (2014).

[58] T. Takayama, A. N. Yaresko, A. S. Gibbs, K. Ishii, D. Kukusta, and H. Takagi, Phys. Rev. Materials **4**, 075002 (2020).

[59] Y. Wang, G. Fabbris, M. Dean, and G. Kotliar, Comput. Phys. Commun. **243**, 151 (2019).

[60] J. G. Vale, C. D. Dashwood, E. Paris, L. S. I. Veiga, M. Garcia-Fernandez, A. Nag, A. Walters, K.-J. Zhou, I.-M. Pietsch, A. Jesche, P. Gegenwart, R. Coldea, T. Schmitt, and D. F. McMorrow, Phys. Rev. B **100**, 224303 (2019).

[61] B. Yuan, J. P. Clancy, A. M. Cook, C. M. Thompson, J. Greedan, G. Cao, B. C. Jeon, T. W. Noh, M. H. Upton, D. Casa, T. Gog, A. Paramekanti, and Y.-J. Kim, Phys. Rev. B **95**, 235114 (2017).

[62] Y. Li, S. M. Winter, D. A. S. Kaib, K. Riedl, and R. Valenti, Phys. Rev. B **103**, L220408 (2021).

[63] A. V. Kolobov, A. Rogalev, F. Wilhelm, N. Jaouen, T. Shima, and J. Tominaga, Appl. Phys. Lett. **84**, 1641 (2004).

[64] D. I. Khomskii, K. I. Kugel, A. O. Sboychakov, and S. V. Streltsov, J. Exp. Theor. Phys. **122**, 484 (2016).

[65] N. Nagasundaram and A. Francis, J. Phys. Chem. Solids **50**, 163 (1989).

[66] F. Gel'mukhanov, T. Privalov, and H. Ågren, Phys. Rev. B **62**, 13996 (2000).

[67] D. Pillay, M. D. Johannes, I. I. Mazin, and O. K. Andersen, Phys. Rev. B **78**, 012501 (2008).

[68] K. I. Kugel, D. I. Khomskii, A. O. Sboychakov, and S. V. Streltsov, Phys. Rev. B **91**, 155125 (2015).

[69] E. Lefrançois, A.-M. Pradipto, M. Moretti Sala, L. C. Chapon, V. Simonet, S. Picozzi, P. Lejay, S. Petit, and R. Ballou, Phys. Rev. B **93**, 224401 (2016).

[70] M. Rossi, M. Retegan, C. Giacobbe, R. Fumagalli, A. Efimenko, T. Kulka, K. Wohlfeld, A. I. Gubanov, and M. Moretti Sala, Phys. Rev. B **95**, 235161 (2017).

[71] A. Paramekanti, D. J. Singh, B. Yuan, D. Casa, A. Said, Y.-J. Kim, and A. D. Christianson, Phys. Rev. B **97**, 235119 (2018).

[72] X. Ming, X. Wan, C. Autieri, J. Wen, and X. Zheng, Phys. Rev. B **98**, 245123 (2018).

[73] A. A. Aczel, J. P. Clancy, Q. Chen, H. D. Zhou, D. Reig-i-Plessis, G. J. MacDougall, J. P. C. Ruff, M. H. Upton, Z. Islam, T. J. Williams, S. Calder, and J.-Q. Yan, Phys. Rev. B **99**, 134417 (2019).